Biostatistics (2021) **22**, 3, *pp.* 613–628
doi:10.1093/biostatistics/kxz056
Advance Access publication on December 27, 2019

Mapping epileptic directional brain networks using intracranial EEG data

HUAZHANG LI†, YAOTIAN WANG†, SEIJI TANABE, YINGE SUN, GUOFEN YAN, MARK S. QUIGG, TINGTING ZHANG*

Department of Statistics, University of Virginia 148 Amphitheater Way, Charlottesville, VA 22904-4135, USA

tz3b@virginia.edu

Summary

The human brain is a directional network system, in which brain regions are network nodes and the influence exerted by one region on another is a network edge. We refer to this directional information flow from one region to another as *directional connectivity*. Seizures arise from an epileptic directional network; abnormal neuronal activities start from a seizure onset zone and propagate via a network to otherwise healthy brain regions. As such, effective epilepsy diagnosis and treatment require accurate identification of directional connections among regions, i.e., mapping of epileptic patients' brain networks. This article aims to understand the epileptic brain network using intracranial electroencephalographic data—recordings of epileptic patients' brain activities in many regions. The most popular models for directional connectivity use ordinary differential equations (ODE). However, ODE models are sensitive to data noise and computationally costly. To address these issues, we propose a high-dimensional state-space multivariate autoregression (SSMAR) model for the brain's directional connectivity. Different from standard multivariate autoregression and SSMAR models, the proposed SSMAR features a cluster structure, where the brain network consists of several clusters of densely connected brain regions. We develop an expectation–maximization algorithm to estimate the proposed model and use it to map the interregional networks of epileptic patients in different seizure stages. Our method reveals the evolution of brain networks during seizure development.

Keywords: Brain networks; Directional connectivity; Dynamic system; EM algorithm.

1. Introduction

The human brain is a network system consisting of many interacting regions; brain regions are network nodes, and the directional effect exerted by one region over another corresponds to a directional network edge in the brain network. This directional information passed by one region to another is referred to as directional connectivity.

Understanding how the interregional network is related to the functions and dysfunctions of the brain is one of the central goals of neuroscience. We here focus on mapping the normal and abnormal brain

*To whom correspondence should be addressed.
†These authors are the co-first authors.

networks of epileptic patients using intracranial electroencephalography (iEEG) recordings of their brain activities. Note that directional connectivity is also called effective connectivity (Friston, 2011), which is typically examined under the dynamical causal model (DCM) based on functional magnetic resonance imaging (fMRI) and scalp electroencephalography (EEG) data (Friston *and others*, 2003; Friston, 2009). To emphasize the different data and model used in this article, we call the connectivity under our study directional connectivity.

In a typical focal seizure, abnormal and excessive neural activity starts from the seizure onset zone (SOZ) and propagates to otherwise healthy brain regions. As such, seizures are a directional network phenomenon. Understanding the epileptic brain network is critical to the diagnosis and the treatment of patients who suffer from the inability to control seizures with medication (Devinsky, 1999), also known as drug-resistant epilepsy (DRE). In the epilepsy diagnosis of patients with DRE, neurosurgeons implant electrodes either on the cortex or via depth electrodes to monitor the activities of many moderately small brain regions—a technique called iEEG. The recorded data are multivariate time-series of voltage waveforms, which often exceed 50 channels. Figure 1(a) shows the electrode placement on the left hemisphere of a patient who underwent iEEG recordings in evaluation for epilepsy surgery. Figure 1(b) shows a short 5-s segment of the patient's iEEG recordings in two regions/channels.

In contrast to noninvasive brain activity measurements, e.g., fMRI, EEG, and magnetoencephalography (MEG), each iEEG electrode directly records the neuronal activity in one small region (10 mm in diameter) at a millisecond scale, and iEEG data possess several nice properties, including high spatial resolution, high temporal resolution, and a much stronger signal-to-noise ratio (SNR, Cervenka *and others*, 2013) than EEG and fMRI data.

Previous studies of iEEG data developed quantitative methods to examine epileptic patients' brain networks (Bartolomei *and others*, 2010; David *and others*, 2011; Andrzejak *and others*, 2012). The most popular methods are information-theoretic measures of directional connectivity (Burns *and others*, 2014; Kramer *and others*, 2012). However, these methods typically focus on pairwise relationships between regions and cannot delineate the entire pathway of signal transfer that can transit through more than two regions.

Since the brain is a dynamic system on the time domain, a more effective approach to investigating the brain is to build a dynamic-system model for characterizing simultaneous directional interactions among all the regions under study on the time domain and to estimate the model parameters that quantify directional connectivity. This approach can provide a comprehensive picture of the relationship among all the regions and capture the mechanism of the brain. The most popular dynamic-system models for the brain use ordinary differential equations (ODE) to characterize directional connectivity. These include DCM (Daunizeau *and others*, 2011; David *and others*, 2006) and neural mass models (NMM, Wendling *and others*, 2002) based on fMRI and EEG data. However, DCMs and NMMs are mostly for directional connectivity among only a few brain regions, that is, for low-dimensional brain networks.

For high-dimensional systems, Chen and Wu (2008), Wu *and others* (2014), Zhang *and others* (2015, 2017, 2019) proposed to use linear ODEs to approximate complex interactions among many system components. Despite their simplicity, these high-dimensional ODE models share several other issues with their complex counterparts. First, as deterministic models, ODE models fail to take into account the potential discrepancy between the assumed model and the underlying true dynamical system. Second, the estimates of ODE parameters are sensitive to data noise, because the estimates of derivatives of the state functions of ODEs are highly sensitive to a low data-sampling rate and data noise (Ramsay, 2006). Third, ODE model estimation is computationally expensive.

To address the limitations of ODE models, we propose a state-space multivariate auto-regression (MAR)-based model (SSMAR) for the directional brain network. What separates our model from a standard MAR and SSMAR models (Korzeniewska *and others*, 2011, 2008; Goebel *and others*, 2003) is 2-fold. First, our model, as an approximation of a high-dimensional dynamic system within a short

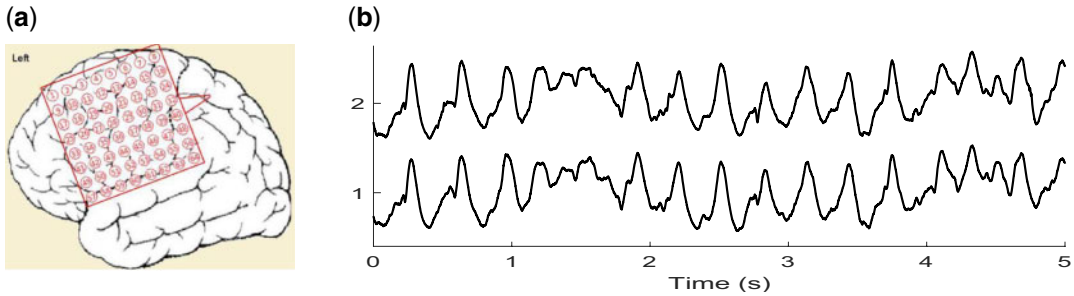

Fig. 1. (a) The iEEG electrode placement on the left hemisphere of an epileptic patient under study. (b) Two channels/electrodes' 5-second iEEG time series.

period of time, does not require stationarity. Second, the proposed high-dimensional model uses a large number of parameters to quantify directional connectivity among many regions. To increase estimation efficiency, our model considers sparse networks, especially those in a cluster structure (Milo *and others*, 2004; Newman, 2006), where subsets of regions have particularly dense connections between themselves, but not to others. The cluster structure fits nicely with the functional specialization of the human brain (Sporns, 2011, pp. 71); the brain areas that are specialized in the same or similar function tend to densely connect with each other to form a cluster (Sporns, 2013). We propose a Potts model (Potts, 1952) for the MAR parameters to incorporate the cluster structure. The ensuing new state-space MAR model with the Potts Model is referred to as the modular state-space multivariate auto-regressive model (MSSMAR).

To estimate the MSSMAR, we propose a penalized log-likelihood criterion, which uses a penalty converted from the Potts model to regularize the size of clusters and to impose the sparsity on the network result. Then, we develop an expectation–maximization (EM) algorithm to optimize the criterion, identify clusters of connected regions, and map brain networks. The EM algorithm uses the Kalman filter and smoother in the expectation step and thus, is computationally fast. We show that the proposed model is more effective than existing methods in identifying connected regions even for data generated from the models different from the assumed SSMAR (Section 4). In summary, this article builds a new dynamic-system model for the brain network and develops a computationally efficient estimation method to identify connected brain regions. Our new method fits well with the brain's functional organization and is robust to various deviations from the assumed model.

The rest of the article is organized as follows. In Section 2, we introduce a general SSMAR and propose the MSSMAR for iEEG data. In Section 3, we propose a log-likelihood-based criterion with the Potts penalty and develop an EM algorithm to maximize the criterion for estimating the MSSMAR. We also discuss a penalty parameter selection method. In Section 4, we use simulation examples to show that the MSSMAR is robust to various violations of model assumptions and outperforms existing popular network methods. In Section 5, we apply the MSSMAR to iEEG data of an epileptic patient and reveal changes from the normal brain network to abnormal one as the seizure develops. Section 6 discusses future research directions.

2. A DYNAMIC MODEL FOR IEEG DATA

2.1. *The state-space MAR model*

Let $\boldsymbol{y}(t) = (y_1(t), \ldots, y_d(t))'$ be the observed iEEG measurements of d brain regions' neuronal activities at time t for $t = 1, \ldots, T$, where T is the number of iEEG time points to be analyzed. Since brain regions are interacting with each other through neuron firing, the model for directional connectivity should be

constructed at the neuronal states of the regions. We use $\boldsymbol{x}(t) = (x_1(t), \ldots, x_d(t))'$ to represent the d brain regions' neuronal state functions at time t.

Motivated by the DCM (Friston *and others*, 2003), which is a state-space model, we propose a state-space model for $\boldsymbol{y}(t)$. The observation model, i.e., the state model, links $\boldsymbol{y}(t)$ to $\boldsymbol{x}(t)$, and the space model for $\boldsymbol{x}(t)$ characterizes the directional connectivity among d regions.

Since each iEEG electrode directly records one region's neuronal activity with a high spatial resolution and a high SNR, we propose a simple observation model for $\boldsymbol{y}(t)$:

$$y_i(t) = c_i \cdot x_i(t) + \epsilon_i(t), \quad t = 1, \ldots, T, \tag{2.1}$$

where c_i is an unknown constant, and $\epsilon_i(t)$ is a data measurement error with mean zero.

The most common discrete-time dynamic system model in statistics is the multivariate auto-regressive model (MAR). We propose to use the simplest first-order MAR to characterize the directional connectivity among d regions at the neuronal state:

$$x_i(t) = \sum_{j=1}^{d} A_{ij} \cdot x_j(t-1) + \eta_i(t), \tag{2.2}$$

where A_{ij} quantifies the directional connection from region j to region i, and $\eta_i(t)$ is a model error with mean zero. The model error characterizes the variation of $x_i(t)$ that cannot be explained by the model.

The observation model (2.1) and the state model (2.2) together are the proposed state-space MAR (SSMAR) for the brain's directional connectivity. The SSMAR with the separate data measurement error and model error has the model flexibility to approximate different network systems as well as robustness to violations of model assumptions.

We use the first-order SSMAR rather than higher-order ones for two reasons. First, due to the current limited understanding of the human brain, it is impossible to build a high-dimensional model that can explain all the complex temporal activities of many brain regions. Instead, our goal is to identify connected brain regions through detecting the existence of temporal dependence among regions' time series data. Though the first-order MAR may not capture all the temporal dependence among regions, it is effective to capture the major dependence, especially within a short time segment. Second, for the high-dimensional network under study, the first-order MAR uses much fewer parameters than its higher-order counterparts to characterize directional connectivity, which brings estimation efficiency.

Because c_i in (2.1) and the variance of $\eta_i(t)$ are not uniquely defined, we let $(c_1, \ldots, c_d)$ be unknown and assume that the variances of $\eta_i(t)$s all equal 1 to avoid the identifiability issue. We also assume independence among $\boldsymbol{\eta}(t) = (\eta_1(t), \ldots, \eta_d(t))'$, i.e., $\boldsymbol{\eta}(t) \sim \text{MVN}(\mathbf{0}, \mathbf{I})$, where MVN stands for a multivariate normal, and $\mathbf{I}$ is the identity matrix. The independence assumption is to keep the proposed model parsimonious. Again, the goal here is to develop a model that can effectively detect existence of temporal dependence among regions' iEEG data instead of capturing all the spatial and temporal variation of the data. For similar reasons, we assume that the initiate state $\boldsymbol{x}(0) \sim \text{MVN}(\boldsymbol{\mu}_0, \mathbf{I})$ and the model measurement error $\boldsymbol{\epsilon}(t) = (\epsilon_1(t), \ldots, \epsilon_d(t))' \sim \text{MVN}(\mathbf{0}, \mathbf{R})$, where $\mathbf{R}$ is a d by d diagonal variance–covariance matrix.

2.2. *The modular state-space MAR model*

Under the SSMAR, evaluating directional connectivity among d regions is equivalent to estimating d^2 parameters A_{ij}s. For a large d, conventional estimates of the many model parameters have large variances. To increase estimation efficiency, we assume sparsity for the model parameters that denote directional connectivity among regions. However, simple sparsity does not solve the problem. This is because sparse networks can have many different forms, most of which do not correctly represent the brain's functional

organization. For example, typical L_1 regularization-induced sparsity (Basu and Michailidis, 2015; Davis *and others*, 2016; Nicholson *and others*, 2017) implies that every region has very few connections with other regions. However, this network does not fit the brain's functional organization in which regions performing the same or similar functions tend to densely connect with each other.

We assume that the underlying network has a cluster structure for three reasons. First, the cluster structure, consisting of several separate clusters of densely connected regions, fits well with the brain's functional specialization: the brain regions specialized in the same or related function tend to be closely connected. For example, regions responsive to an auditory stimulus are densely connected to form a cluster (Cheung *and others*, 2016). Second, the existing literature on brain networks has widely reported the cluster structure (Newman, 2006; Sporns, 2011). Third, identifying the cluster that includes the SOZ will be useful for neurologists to evaluate the effect of seizures on brain functions because intuitively, regions in the same cluster as the SOZ are those affected by the SOZ's activities most. Considering all these reasons, we propose to incorporate the cluster structure into the SSMAR.

We introduce cluster labels for d brain regions. Let m_i be region i's cluster label, which takes an integer value between 1 and d. The new state model is

$$x_i(t) = \sum_{j=1}^{d} \delta(m_i, m_j) \cdot A_{ij} \cdot x_j(t-1) + \eta_i(t), \tag{2.3}$$

where the Kronecker delta function, $\delta(m_i, m_j)$, equals 1 if $m_i = m_j$ and 0 otherwise.

We refer to equations (2.1) and (2.3) as the modular state-space multivariate autoregressive model (MSSMAR). Under the MSSMAR, we focus on identifying the clusters of closely connected regions.

3. Model estimation

We use $\mathbf{Y}$ to denote all the observed time-series data $\{\boldsymbol{y}(1), \ldots, \boldsymbol{y}(T)\}$ and use $\mathbf{X}$ to denote the underlying state functions $\{\boldsymbol{x}(0), \boldsymbol{x}(1), \ldots, \boldsymbol{x}(T)\}$ of d regions at all the time points. Let $\mathbf{A}$ be a $d \times d$ matrix with entries A_{ij}, $i,j = 1, \ldots, d$, $\boldsymbol{m} = (m_1, \ldots, m_d)'$, and $\boldsymbol{c} = (c_1, \ldots, c_d)'$. The parameters to be estimated in the MSSMAR are $\boldsymbol{\Theta} = \{\boldsymbol{\theta}, \boldsymbol{m}\}$, where $\boldsymbol{\theta} = \{\mathbf{A}, \boldsymbol{c}, \mathbf{R}, \boldsymbol{\mu}_0\}$.

3.1. *Optimization function with the Potts penalty*

We propose to estimate $\boldsymbol{\Theta}$ by maximizing a penalized log-likelihood of $\mathbf{Y}$:

$$PL(\boldsymbol{\Theta}|\mathbf{Y}) = \log(P(\mathbf{Y}|\boldsymbol{\Theta})) - \lambda \cdot \sum_{i=1}^{d} \sum_{j=1}^{d} \delta(m_i, m_j), \tag{3.1}$$

where λ is a positive constant and

$$P(\mathbf{Y}|\boldsymbol{\Theta}) \propto \int P(\boldsymbol{x}(0)|\boldsymbol{\Theta}) \prod_{t=1}^{T} P(\boldsymbol{x}(t)|\boldsymbol{x}(t-1), \boldsymbol{\Theta}) P(\boldsymbol{y}(t)|\boldsymbol{x}(t), \boldsymbol{\Theta}) \, \mathrm{d}\mathbf{X}.$$

The penalty $-\lambda \cdot \sum_{i=1}^{d} \sum_{j=1}^{d} \delta(m_i, m_j)$ is motivated from the Potts model (Potts, 1952) for the cluster labels $\boldsymbol{m} = \{m_1, \ldots, m_d\}$:

$$\mathcal{P}(\boldsymbol{m}) \propto \exp\{-\lambda \cdot \sum_{i=1}^{d} \sum_{j=1}^{d} \delta(m_i, m_j)\}. \tag{3.2}$$

The Potts model (3.2) assigns a small weight to the cluster structure containing large clusters and many connected brain regions. We take the logarithm of the Potts model and use it as a penalty to regularize the size of clusters and to induce a sparse network result.

3.2. *The EM algorithm*

The most popular approach to finding the maximum likelihood estimate (MLE) for the SSMAR (2.1) and (2.2) is the EM algorithm (Holmes *and others*, 2012), because the conditional distribution of $\mathbf{X}$ given $\boldsymbol{\Theta}$ is multivariate normal, and it is straightforward to treat $\mathbf{X}$ as missing data in the EM algorithm. Given this, we develop an EM algorithm to find the maximizer for $PL(\boldsymbol{\Theta}|\mathbf{Y})$.

The EM algorithm iterates between the following two steps.

$$\text{Expectation: } R(\boldsymbol{\Theta}|\boldsymbol{\Theta}^{s-1},\mathbf{Y}) \equiv \mathbb{E}_{\mathbf{X}|\boldsymbol{\Theta}^{s-1},\mathbf{Y}} \log P(\mathbf{X},\mathbf{Y}|\boldsymbol{\Theta}), \tag{3.3}$$

$$\text{Maximization: } \boldsymbol{\Theta}^{s} = \text{argmax}_{\boldsymbol{\Theta}} Q(\boldsymbol{\Theta}|\boldsymbol{\Theta}^{s-1},\mathbf{Y}), \tag{3.4}$$

where $Q(\boldsymbol{\Theta}|\boldsymbol{\Theta}^{s-1},\mathbf{Y}) = R(\boldsymbol{\Theta}|\boldsymbol{\Theta}^{s-1}) - \lambda \cdot \sum_{i=1}^{d}\sum_{j=1}^{d}\delta(m_i,m_j)$.

The conditional distribution of $\mathbf{X}$ given $\mathbf{Y}$ and $\boldsymbol{\Theta}$ is a multivariate normal, so we can use the Kalman filter (Kalman, 1960) and smoother to solve the expectation step (3.3). See details in the Supplementary material available at *Biostatistics* online.

The maximization in (3.4) is an non-deterministic polynomial-time (NP) hard problem because the Potts penalty is an L_0 penalty on the number of nonzero parameters. To address this computational difficulty in finding the maximizer of $Q(\boldsymbol{\Theta}|\boldsymbol{\Theta}^{s-1},\mathbf{Y})$, we use a generalized EM (GEM) algorithm (Neal and Hinton, 1998) to solve the maximization step. The GEM ensures that $Q(\boldsymbol{\Theta}^{s}|\boldsymbol{\Theta}^{s-1}) > Q(\boldsymbol{\Theta}^{s-1}|\boldsymbol{\Theta}^{s-1})$ (Little and Rubin, 2019). Thus, the optimization target function $PL(\boldsymbol{\Theta}|\mathbf{Y})$ increases after every iteration of the GEM algorithm, and the algorithm always converges. Specifically, instead of finding the optimal updates of all regions' cluster labels that maximize $Q(\boldsymbol{\Theta}|\boldsymbol{\Theta}^{s-1},\mathbf{Y})$ (which is an NP hard problem), we update the cluster label of one region only in each maximization step (which is computationally feasible). The details are given below.

Let $\boldsymbol{\theta}^{s-1}$ denote the estimate of $\boldsymbol{\theta}$ after the $(s-1)$th iteration and $\boldsymbol{m}^{s-1} = \{m_1^{s-1},\ldots,m_d^{s-1}\}$, the cluster labels of d regions at step $s-1$. We let $\boldsymbol{m}^0 = \{1,\ldots,d\}$, $\boldsymbol{c}^0 = \{1,\ldots,1\}$, $\boldsymbol{\mu}_0^0 = \mathbf{Y}$, $\mathbf{R}^0 = \mathbf{I}$, and $\mathbf{A}^0$ be the estimates of $\mathbf{A}$ by directly fitting a simple first-order MAR to the data. For each region $i = 1,\ldots,d$, let $\boldsymbol{m}_{-i}^{s-1} = \{m_1^{s-1},\ldots,m_{i-1}^{s-1},m_{i+1}^{s-1},\ldots,m_d^{s-1}\}$. The maximization at the sth step of the GEM is as follows.

A Repeat the following procedure for every region i.
  A.1 Calculate $\max_{m_i,\boldsymbol{\theta}} Q(m_i,\boldsymbol{\theta},\boldsymbol{m}_{-i}^{s-1}|\boldsymbol{\Theta}^{s-1},\mathbf{Y})$ and denote the ensuing value by H_i^s and the ensuing maximizer $(m_i,\boldsymbol{\theta})$ by $(z_i^s,\tilde{\boldsymbol{\theta}}_i^s)$.

B Select the region l whose associated $H_l^s = \max(H_1^s,\ldots,H_d^s)$.

C Let $\boldsymbol{m}_{-l}^s = \boldsymbol{m}_{-l}^{s-1}$, $m_l^s = z_l^s$, and $\boldsymbol{\theta}^s = \tilde{\boldsymbol{\theta}}_l^s$. That is, in the sth maximization step, the optimal one-region cluster-label update is for region l. Then the other $d-1$ regions' cluster labels $\boldsymbol{m}_{-l}^s$ at the sth step are the same as those in the previous step, and region l's cluster label m_l^s and the parameter values $\boldsymbol{\theta}^s$ equal to $(z_l^s,\tilde{\boldsymbol{\theta}}_l^s)$ that maximize $Q(m_i,\boldsymbol{\theta},\boldsymbol{m}_{-i}^{s-1}|\boldsymbol{\Theta}^{s-1},\mathbf{Y})$ given $\boldsymbol{m}_{-i}^{s-1}$ from the previous step.

In the step A.1, to obtain the maximized value H_i^s, we calculate $\max_{\boldsymbol{\theta}} Q(\boldsymbol{\theta},m_i = z,\boldsymbol{m}_{-i}^{s-1}|\boldsymbol{\Theta}^{s-1},\mathbf{Y})$ for every possible value z of m_i (including for $z = m_i^{s-1}$). This calculation is computationally feasible because m_i can take at most $d-1$ different values, and $\max_{\boldsymbol{\theta}} Q(\boldsymbol{\theta},\boldsymbol{m}|\boldsymbol{\Theta}^{s-1},\mathbf{Y})$ has an analytical solution given $\boldsymbol{m}$. Then $H_i^s = \max_z \max_{\boldsymbol{\theta}} Q(\boldsymbol{\theta},m_i = z,\boldsymbol{m}_{-i}^{s-1}|\boldsymbol{\Theta}^{s-1},\mathbf{Y})$ and $z_i^s = \text{argmax}_z \max_{\boldsymbol{\theta}} Q(\boldsymbol{\theta},m_i = z,\boldsymbol{m}_{-i}^{s-1}|\boldsymbol{\Theta}^{s-1},\mathbf{Y})$.

Because the maximization step includes the evaluation of $\max_{\boldsymbol{\theta}} Q(\boldsymbol{\theta}, \boldsymbol{m}^{s-1}|\boldsymbol{\Theta}^{s-1}, \mathbf{Y})$ (which is no smaller than $Q(\boldsymbol{\theta}^{s-1}, \boldsymbol{m}^{s-1}|\boldsymbol{\Theta}^{s-1}, \mathbf{Y})$), the chosen $\boldsymbol{\theta}^s$ and $\boldsymbol{m}^s$ must satisfy $Q(\boldsymbol{\theta}^s, \boldsymbol{m}^s|\boldsymbol{\Theta}^{s-1}, \mathbf{Y}) \geq Q(\boldsymbol{\theta}^{s-1}, \boldsymbol{m}^{s-1}|\boldsymbol{\Theta}^{s-1}, \mathbf{Y})$. As such, the new parameters $\boldsymbol{\theta}^s$ and $\boldsymbol{m}^s$ increase the optimization function $PL(\boldsymbol{\Theta}|\mathbf{Y})$ (Gelman *and others*, 2013; Little and Rubin, 2019).

Though m_i is not identifiable, the regions in the same cluster are unique. The proposed algorithm does not experience the cluster label switch over iterations. This is because the maximization step guarantees that the value of the objective function monotonically increases, while the cluster label switch does not increase the optimization function.

3.3. *Penalty parameter selection*

The penalty parameter λ regularizes the size of the clusters in the brain network and determines the sparsity level of the network results. We propose to use the Akaike information criterion (AIC) to select λ. However, for the proposed high-dimensional model with many free parameters, AIC tends to pick small λs that lead to many nonzero model parameters, that is, AIC tends to overfit (Claeskens and Hjort, 2008). To address this issue, we first exclude λs that result in networks with large clusters, as explained in detail below.

We first determine the upper bound 2^U for λ, where U is a positive integer. We apply the developed EM algorithm with each of $\lambda \in \{2^u, u = 1, 2, ...\}$ to the data $\mathbf{Y}$. The smallest $\lambda \in \{2^u, u = 1, 2, ...\}$ that leads to a network with d clusters is the upper bound. For each candidate $\lambda \in \{0, 0.1, 0.2, \ldots, 2^U\}$ (or $\{0, 0.01, 0.02, \ldots, 2^U\}$ if $U = 1$), we apply the developed EM algorithm to $\mathbf{Y}$ and obtain the ensuing network results.

We exclude λs that lead to networks with too large clusters or too many small clusters, specifically, networks whose largest cluster contains more than 50% or fewer than 10% of d regions. We found that if the largest cluster contains more than 50% of regions, more than 25% of model parameters are nonzero, resulting in non-sparse networks. If the largest cluster contains fewer than 10% of d regions, the ensuing network has too many small clusters and is difficult to interpret scientifically.

We use the AIC to select λ among the rest of the parameters. The AIC is defined as

$$\mathrm{AIC}(\lambda) = -2\log\left(P(\mathbf{Y}|\hat{\boldsymbol{\Theta}})\right) + 2\sum_{1\leq i<j\leq d}\delta(\hat{m}_i, \hat{m}_j),$$

where $\hat{\boldsymbol{\Theta}}$ is the output of the EM algorithm. Since the first screening step excludes most λs that very likely lead to overfitting, the AIC can select λ with a low false positive rate (FPR), as demonstrated in the simulation study. Moreover, since it is straightforward to evaluate the AIC at the end of the EM algorithm, the second step of AIC-based penalty parameter selection does not require additional computation for each candidate λ. In summary, the proposed penalty selection procedure is computationally fast and easy to implement.

4. Simulation study

4.1. *Comparison with ODE models*

The most popular dynamic system models for the brain's directional connectivity use ODEs to describe the biophysical interactions among usually only a few brain regions (Friston *and others*, 2003). Zhang *and others* (2019) proposed a high-dimensional second-order ODE model to characterize directional connectivity of a high-dimensional brain network and to simultaneously accommodate brain regions' oscillatory activities, a rhythmic or repetitive neural activity involved in many brain

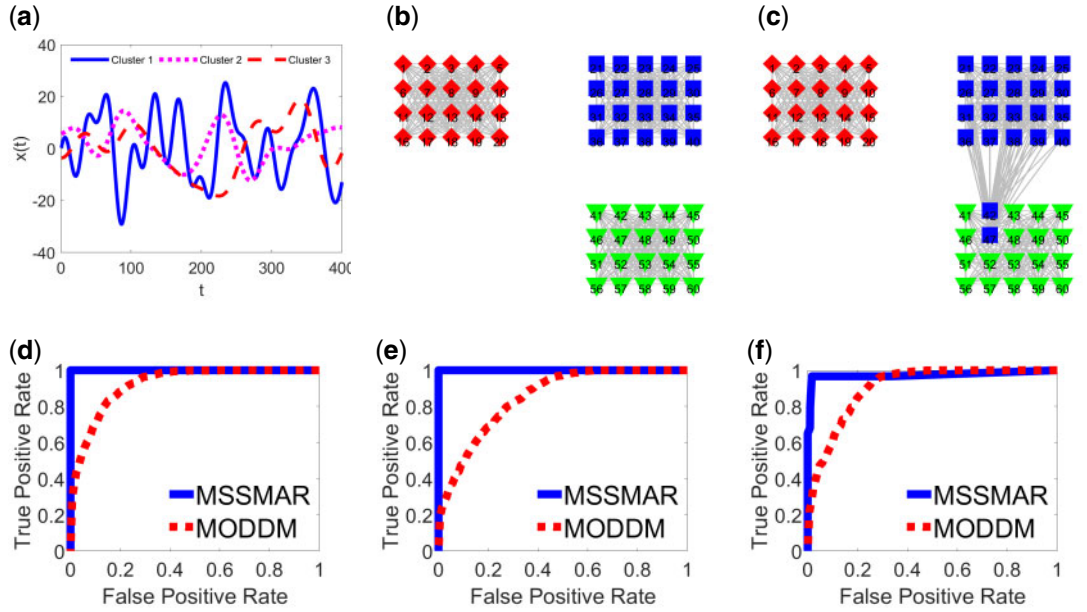

Fig. 2. (a) Simulated $\boldsymbol{x}(t)$ of three regions in three different clusters. (b) The true network of the simulated system. (c) The estimated network for 200 Hz data. Nodes of the same shape (square, triangle, or diamond) correspond to the regions identified to be in the same cluster. Each line indicates one pair of directionally connected regions. (d)–(f) ROC curves of identifying connected regions by the proposed MSSMAR and an MODDM-based method for data with temporal resolutions 800 Hz, 400 Hz, and 200 Hz, respectively.

functions (Fell and Axmacher, 2011). The ODE model is

$$\frac{\mathrm{d}^2 x_i(t)}{\mathrm{d}t^2} = \sum_{j=1}^{d} \delta(m_i, m_j) \cdot A_{ij} \cdot x_j(t) + D_i + G_i \frac{\mathrm{d}x_i(t)}{\mathrm{d}t}. \tag{4.1}$$

The above model is referred to as the modular oscillatory dynamic directional model (MODDM).

We use the data generated from the above ODE model to examine the robustness and effectiveness of our method in identifying connected regions and compare the ensuing network results with those of ODE approaches. We generated $d = 60$ state functions $\boldsymbol{x}(t)$ from the model (4.1) using discretization methods (Campbell, 2007; Cao *and others*, 2012; Xue *and others*, 2010). The simulated system has three clusters, each consisting of 20 pairwise connected regions. The simulated $\boldsymbol{x}(t)$, shown in Figure 2(a), have oscillatory patterns similar to the iEEG time series in Figure 1(b). Figure 2(b) shows the true network among the 60 regions. Nodes of the same shape (square, triangle, or diamond) correspond to the regions in the same cluster. Each line indicates the existence of a directional connection between the two regions at the two ends of the line.

We generated measurement errors $\epsilon_i(t)$ from the following model:

$$\boldsymbol{\epsilon}(t) = 0.5\boldsymbol{\epsilon}(t-1) + \boldsymbol{\zeta}(t) \text{ and } \boldsymbol{\zeta}(t) \overset{i.i.d}{\sim} \mathrm{MVN}(0, \mathbf{D}^{\frac{1}{2}} \boldsymbol{\Sigma}_1 \mathbf{D}^{\frac{1}{2}}), \tag{4.2}$$

where $\boldsymbol{\Sigma}_1$ is a block diagonal matrix with each block corresponding to one cluster. We let all the diagonal entries of $\boldsymbol{\Sigma}_1$ be 1 and sampled the off-diagonal entries in each block independently from Unif(0, 0.5).

We chose 0.5 to be the upper bound for off-diagonal entries such that $\mathbf{\Sigma}_1$ is strictly positive definite. The matrix $\mathbf{D}$ is a diagonal matrix whose diagonal entries were chosen such that the SNR of $y_i(t)$, defined as $\text{var}(x_i(t))/\text{var}(\epsilon_i(t))$, is 10, mimicking the strong SNR of the real data (Zhang *and others*, 2015). As such, $\boldsymbol{\epsilon}(t)$ is spatially (among regions) and temporally correlated.

The sum of $x_i(t)$ and $\epsilon_i(t)$ yields $y_i(t)$. We produced $\boldsymbol{y}(t)$ of three different temporal resolutions, 800 Hz (800 equally spaced time points observed each second), 400 Hz, and 200 Hz, and applied the MSSMAR to the three sets of time series with three different frequencies independently.

We applied the proposed MSSMAR to $\boldsymbol{y}(t)$ using different penalty parameters λ. With each penalty parameter, we identified connected brain regions and calculated the ensuing true positive rate (TPR) and FPR. Figures 2(d–f) show the ROC curves, i.e., pairs of TPRs vs. FPRs, of network edge selection (i.e., selection of connected regions) by the MSSMAR for data of frequencies 800 Hz, 400 Hz, and 200 Hz, respectively. We also found that the network results by using the penalty parameter λ selected by the AIC were almost identical to the true network. Figure 2(c) shows the network result for the 200-Hz data, which has a TPR of 93.7% and FPR of 3.3%.

For comparison, we examined the ROC curves (dotted lines) of a method directly based on the assumed MODDM (4.1) (Zhang *and others*, 2019). The results show that the ODE-based method is sensitive to data noise and most effective for high-frequency data. In contrast, the proposed MSSMAR is robust to data noise and low data-sampling rates and outperforms the ODE-based method with much higher TPRs given the same FPRs, even for data generated from the assumed ODE models.

4.2. *Comparison with high-order SSMARs*

In multivariate time series analysis, higher-order SSMARs are usually more popular than the first-order SSMAR, as the former can better capture complex spatial and temporal dependence among multivariate time series data. We claim that even for time series from high-order SSMARs, the proposed MSSMAR is still efficient in detecting connected brain regions. To demonstrate this, we simulated data from the following third-order SSMAR.

$$x_i(t) = \sum_{j=1}^{d} A_{1,ij} \cdot x_j(t-1) + \sum_{j=1}^{d} A_{2,ij} \cdot x_j(t-2) + \sum_{j=1}^{d} A_{3,ij} \cdot x_j(t-3) + \eta_i(t),$$

$$y_i(t) = x_i(t) + \epsilon_i(t),$$

where $d = 50$. Region j has a directional effect over region i if at least one of $A_{1,ij}, A_{2,ij}$, and $A_{3,ij}$ is nonzero. The simulated system consists of three clusters of size 15, 15, and 20 and has both within-cluster and between-cluster connections. All the regions in the same cluster are pairwise connected, and the between-cluster connections are much sparser than within-cluster connections. Figure 3(a) shows the simulated network of the system.

We simulated the state model errors $\boldsymbol{\eta}(t) = (\eta_1(t), \ldots, \eta_d(t))'$ from the model

$$\boldsymbol{\eta}(t) = 0.5\boldsymbol{\eta}(t-1) + \boldsymbol{\delta}(t) \text{ and } \boldsymbol{\delta}(t) \overset{i.i.d}{\sim} \text{MNV}(0, \mathbf{\Sigma}_2), \tag{4.3}$$

where $\mathbf{\Sigma}_2$ is created in the same way as $\mathbf{\Sigma}_1$. We generated the observation errors $\boldsymbol{\epsilon}(t)$ from the model (4.2) and set the SNR to be 10. As such, both the state model errors $\boldsymbol{\eta}(t)$ and data measurement errors $\boldsymbol{\epsilon}(t)$ are spatially (among regions) and temporally correlated.

We compare the MSSMAR with four existing network methods, including the MAR with an L_1 penalty (MAR(L_1)) by using the R package BigVAR, partial directed coherence (PDC) (Baccalá and Sameshima, 2001), spectral synchrony (Euán *and others*, 2018), and graphical Lasso (Glasso) (Friedman *and others*,

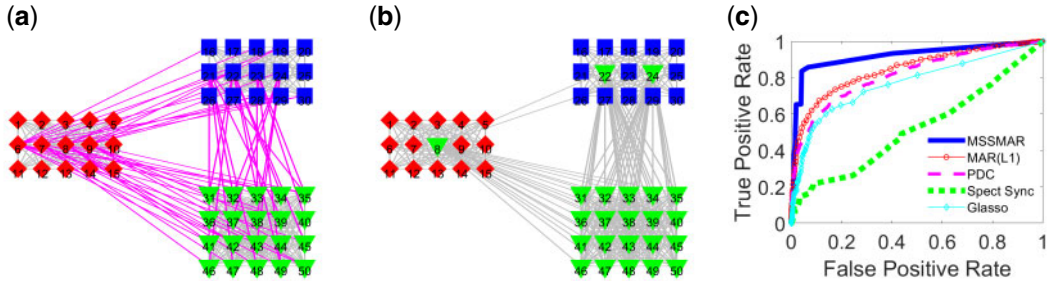

Fig. 3. (a) The true network of the generated system. (b) The estimated network by the MSSMAR. Nodes of the same shape (square, triangle, or diamond) correspond to the regions identified to be in the same cluster. Each line indicates one pair of connected regions. (c) ROC curves of the proposed method and competing methods, including the MAR with an L_1 penalty (MAR(L1)), partial directed coherence (PDC), spectral synchrony, and graphical Lasso (Glasso).

2014; Witten *and others*, 2011). We used different penalty parameters or thresholds for the five methods, calculated the ensuing TPRs and FPRs, and plotted the ROC curves of the five methods in Figure 3(c). Despite that the assumed MSSMAR deviates from the data generating model both in terms of the relationship among regions and the distributions of error terms, the MSSMAR achieves the highest accuracy in selecting network edges and outperforms all the other four competing methods.

Figure 3(a) shows the estimated network by the MSSMAR with the selected penalty parameter. The estimated network has a TPR of 85.8% and FPR of 6.7%. Three brain regions that have between-cluster connections were classified into a wrong cluster. Nevertheless, the MSSMAR correctly clustered the other 47 regions. In summary, due to distinct densities of within-cluster and between-cluster connections, the proposed MSSMAR can identify clusters and connected regions with high accuracy.

5. ANALYSIS OF EPILEPTIC PATIENT'S IEEG DATA

We used the proposed MSSMAR to examine brain networks of an epileptic patient who underwent iEEG monitoring for epilepsy surgery evaluation. Figure 1(a) shows the electrode placement on the left hemisphere of the patient. The iEEG recordings captured the patient's brain activities at three seizures. Through visually examining the iEEG data around the seizure onset time, EEG experts determined that channel/region 37 (G37) of the 8×8 grid was the SOZ, the region where seizures start and spread to other regions. Channels 63 and 64, as the reference electrodes, were removed from the analysis. Thus, we evaluated connectivity among the rest 62 regions.

To understand the patient's network changes around the seizure onset, we focused on four time periods: 26–50 s before seizure onset, 1–25 s before seizure onset, 1–25 s after seizure onset, and 26–50 s after seizure onset. Following the common practice in the literature (Burns *and others*, 2014), we applied our developed method to each 1-s iEEG segment of 1000 time points (the temporal resolution is 1000 Hz) independently. This approach ensures effective approximation of the brain system by the MSSMAR. In total, we analyzed 300 1-s segments (4 periods $\times$ 25 s $\times$ 3 seizures).

We used the first 1-s segment in each period to select the penalty parameter for analyzing 75 segments in that period. For each 1-s segment, we obtained a 62×62 connectivity matrix, denoted by $\mathbf{M}$. Its (i, j)th entry $M_{ij} = 1$ indicates regions i and j detected to be in the same cluster; and 0 otherwise. For each period, by analyzing 75 1-s segments separately (25 s $\times$ 3 seizures), we obtained 75 connectivity matrices and calculated the average of 75 M_{ij}s for each pair of regions i and j during that period. We use B_{ij} to denote the average and refer to it as the clustering probability between regions i and j.

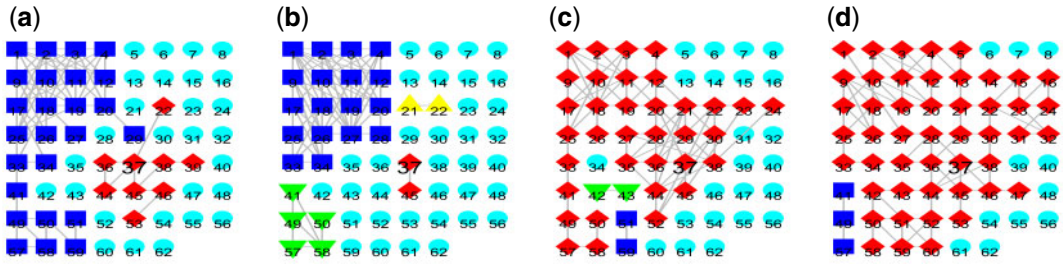

Fig. 4. Brain networks for four periods. $t = 0$ is the starting time of seizure onset. Each gray network edge indicates a pair of brain regions with the top 5% clustering probability. Nodes of the same shape (square, triangle, up-pointing triangle, down-pointing triangle, or diamond) correspond to the regions identified to be in the same cluster. Circles correspond to the regions that have no connection with the other regions. (a) $t \in [-50, -25]$ s, (b) $t \in [-25, 0]$ s, (c) $t \in [0, 25]$ s, and (d) $t \in [25, 50]$ s.

We identify regions to be in the same cluster through giving a threshold to B_{ij}s. For example, if B_{ij} and B_{jk} are above the threshold, regions i, j, and k are deemed in the same cluster regardless whether B_{ik} is above the threshold or not. We select regions with top 5% clustering probabilities. Figures 4(a–d) show the network results by the proposed method for the four periods. An edge indicates that the clustering probability of the two regions in the same cluster is above the threshold. Nodes of the same shape of either square, up-pointing triangle, down-pointing triangle, and diamond correspond to the regions identified to be in the same cluster. Nodes in circles correspond to the regions that have no connection with the other regions.

We found that the epileptic brain network underwent dramatic changes at the time of seizure initiation and propagation. The networks for the two pre-seizure periods were similar (Figures 4(a) and (b)), indicating that the subject's interregional network was stable before seizure onset. However, once seizures started, more regions became connected (Figure 4(c)). Addition continued as seizures further developed (Figure 4(d)).

We identified several clusters. The regions in the same cluster tended to be in spatial proximity, even though spatial proximity was never regularized in the estimation. This result is in line with existing findings that spatially close small regions tend to have similar functions and thus, supports our approach of imposing the cluster structure on the model parameters.

The SOZ (G37) mainly connected to its a few neighboring regions prior to seizure onset (Figures 4(a) and (b)). The SOZ (G37) then became actively engaged in connections with many other regions when seizures started (Figure 4(c)). As the seizure further developed, more and more regions fell into the same cluster as the SOZ, as evidenced by the expansion of brain regions indicated by spade (Figure 4(d)).

In summary, the analysis results are in line with the literature of the focal seizures: abnormal brain activities start from the SOZ and spread to other regions, resulting in excessively synchronous neuronal activity of many regions or the whole brain (Kutsy *and others*, 1999). In addition, our method reveals brain network changes during seizure initiation and propagation: as seizures develop, more and more regions are affected by the activity from the SOZ.

For comparison, we mapped the patient's brain networks in the periods right before and right after the seizure onset by using existing network methods, including correlation (Figures 5(a) and (b)), cross-correlation (Figures 5(c) and (d)) (Brazier and Casby, 1952; Kramer *and others*, 2009), MAR(L_1) (Figures 5(e) and (f)), Glasso (Figures 5(g) and (h)), PDC (Figures 5(i) and (j)), and directed transfer function (DTF) (Figures 5(k) and (l)) (Kaminski and Blinowska, 1991). All these methods failed to detect the brain network changes at the seizure onset.

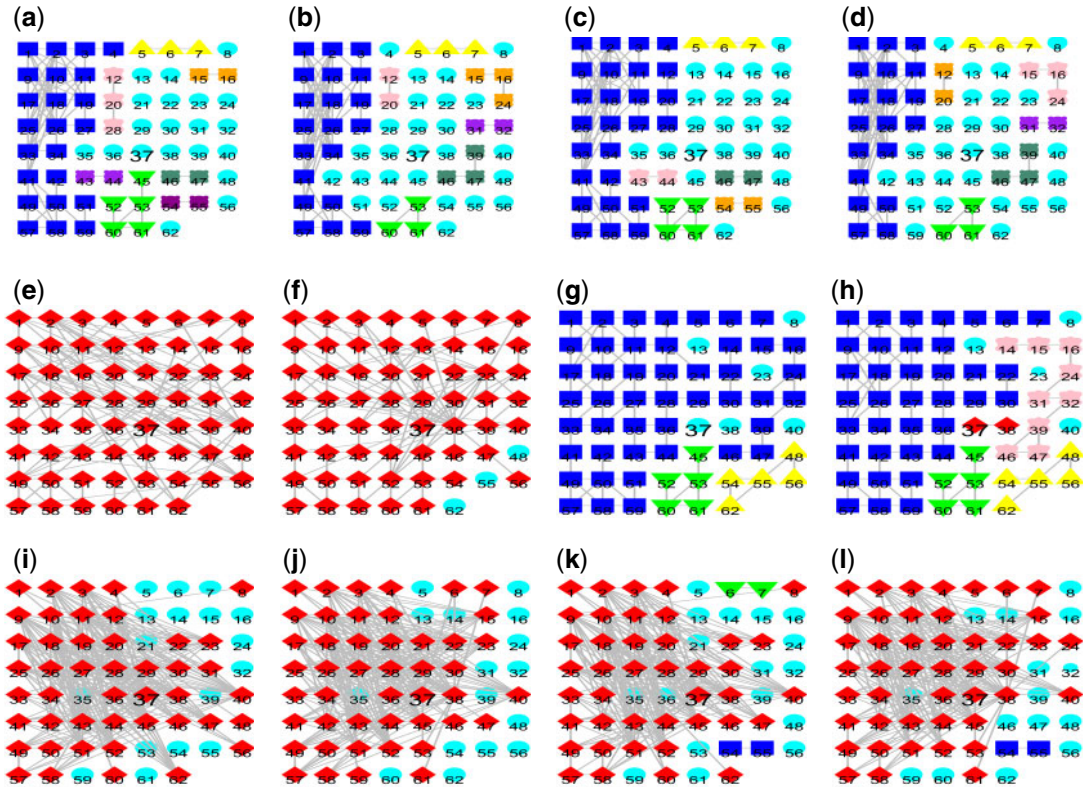

Fig. 5. Brain networks estimated using correlation, cross-correlation, MAR with an L_1 penalty (MAR(L_1)), graphical Lasso (Glasso), partial directed coherence (PDC), and directed transfer function (DTF) methods. Each network edge indicates a pair of regions identified to be connected by the competing methods. (a) Correlation pre-seizure, (b) correlation seizure onset, (c) Cross-Corr. pre-seizure, (d) Cross-Corr. seizure onset, (e) MAR(L_1) pre-seizure, (f) MAR(L_1) seizure onset, (g) Glasso pre-seizure, (h) Glasso onset, (i) PDC pre-seizure, (j) PDC seizure onset, (k) DTF pre-seizure, and (l) DTF seizure onset.

6. DISCUSSION

Identifying connected brain regions and mapping brain networks are challenging because potential patterns of brain networks are enormous. Moreover, the complex spatial–temporal relationship between many brain regions' activities is difficult to specify. To address these challenges, we propose to use a state-space first-order MAR model to approximate the complex brain system and impose the cluster structure on the model parameters to increase efficiency in identifying connected brain regions.

The proposed MSSMAR model is far from being a perfect model of an interregional network. Instead, it is a working model for mapping brain networks of directional connectivity. The model is in clear contrast with ODE models, which are built upon biophysical mechanisms. The MSSMAR model is robust to data noise and low data-sampling rate. With the imposed cluster structure, the proposed method can effectively identify connected regions, especially when information of the brain system under study is incomplete.

We propose to use AIC to select the penalty parameter λ rather than Bayesian information criterion (BIC) because we found that BIC tends to pick large λ that results in overly sparse networks consisting of many small clusters. We suppose this is because the standard BIC, based on the number of data points, $d \cdot T$, overestimates the amount of available data information. Since the multivariate time series data under study

have complex spatial and temporal dependence among recorded regions, the available data information is much less than that of $d \cdot T$ independent data points. To get around the difficulty of accurately evaluating the amount of available data information, we use AIC to select λ.

We did not assume between-cluster connections in the proposed MSSMAR for two reasons. First, the focus of this article is to identify clusters of strongly connected regions, especially the cluster that includes the SOZ for the epilepsy diagnosis. Due to distinct densities of within-cluster and between-cluster connections, our approach could detect clusters even when between-clusters connections exist. Second, the iEEG data under study were from spatially close regions and the strong connections among them are mainly within-cluster connections, which are strong and short-range in contrast to typically long-range between-cluster connections.

Note that though many approaches such as stochastic blockmodels (Airoldi *and others*, 2008; Durante and Dunson, 2014; Geng *and others*, 2018; Nowicki and Snijders, 2001) have been developed in the literature to characterize both within- and between-cluster connections and to identify clusters, these methods are mainly for the networks whose edges are directly observed. In contrast, we here aim to infer the network edges and clusters based on time series measurements of activities of network nodes. Extending the current model to allow for between-cluster connections will lead to a significantly more complex model and requires a new estimation method, which is beyond the scope of the current article. We will address this topic in future research.

Software

Software in the form of MATLAB code is available from https://github.com/StatDeptZhang/Modular-state-space-multivariate-autoregression.

Supplementary material

Supplementary material is available at http://biostatistics.oxfordjournals.org.

Acknowledgments

Conflict of Interest: None declared.

Funding

National Science Foundation-1758095 and the Quantitative Collaborative at the University of Virginia to T.Z.

References

Airoldi, E. M., Blei, D. M., Fienberg, S. E. and Xing, E. P. (2008). Mixed membership stochastic blockmodels. *Journal of Machine Learning Research* **9**, 1981–2014.

Andrzejak, R. G., Schindler, K. and Rummel, C. (2012). Nonrandomness, nonlinear dependence, and nonstationarity of electroencephalographic recordings from epilepsy patients. *Physical Review E* **86**, 046206.

Baccalá, L. A. and Sameshima, K. (2001). Partial directed coherence: a new concept in neural structure determination. *Biological Cybernetics* **84**, 463–474.

Bartolomei, F., Cosandier-Rimele, D., McGonigal, A., Aubert, S., Régis, J., Gavaret, M., Wendling, F. and Chauvel, P. (2010). From mesial temporal lobe to temporoperisylvian seizures: a quantified study of temporal lobe seizure networks. *Epilepsia* **51**, 2147–2158.

BASU, S. AND MICHAILIDIS, G. (2015). Regularized estimation in sparse high-dimensional time series models. *The Annals of Statistics* **43**, 1535–1567.

BRAZIER, M. A. B. AND CASBY, J. U. (1952). Crosscorrelation and autocorrelation studies of electroencephalographic potentials. *Electroencephalography and Clinical Neurophysiology* **4**, 201–211.

BURNS, S. P., SANTANIELLO, S., YAFFE, R. B., JOUNY, C., CRONE, N., BERGEY, G., ANDERSON, W. S. AND SARMA, S. V. (2014). Network dynamics of the brain and influence of the epileptic seizure onset zone. *Proceedings of the National Academy of Sciences of the United States of America* **111**, 5321–5330.

CAMPBELL, D. A. (2007). Bayesian collocation tempering and generalized profiling for estimation of parameters from differential equation models. Montreal: McGill University.

CAO, J., HUANG, J. Z. AND WU, H. (2012). Penalized nonlinear least squares estimation of time-varying parameters in ordinary differential equations. *Journal of Computational and Graphical Statistics* **21**, 42–56.

CERVENKA, M. C., FRANASZCZUK, P. J., CRONE, N. E., HONG, B., CAFFO, B., BHATT, P., LENZ, F. A. AND BOATMAN-REICH, D. (2013). Reliability of early cortical auditory gamma-band responses. *Clinical Neurophysiology* **124**, 70–82.

CHEN, J. AND WU, H. (2008). Efficient local estimation for time-varying coefficients in deterministic dynamic models with applications to HIV-1 dynamics. *Journal of the American Statistical Association* **103**, 369–384.

CHEUNG, C., HAMILTON, L. S., JOHNSON, K. AND CHANG, E. F. (2016). The auditory representation of speech sounds in human motor cortex. *Elife* **5**, e12577.

CLAESKENS, G. AND HJORT, N. L. (2008). Model selection and model averaging. Cambridge: Cambridge University Press.

DAUNIZEAU, J., DAVID, O. AND STEPHAN, K. E. (2011). Dynamic causal modelling: a critical review of the biophysical and statistical foundations. *NeuroImage* **58**, 312–322.

DAVID, O., BLAUWBLOMME, T., JOB, A.-S., CHABARDÈS, S., HOFFMANN, D., MINOTTI, L. AND KAHANE, P. (2011). Imaging the seizure onset zone with stereo-electroencephalography. *Brain* **134**, 2898–2911.

DAVID, O., KIEBEL, S. J., HARRISON, L., MATTOUT, J., KILNER, J. AND FRISTON, K. J. (2006). Dynamic causal modelling of evoked responses in EEG and MEG. *NeuroImage* **30**, 1255–1272.

DAVIS, R. A., ZANG, P. AND ZHENG, T. (2016). Sparse vector autoregressive modeling. *Journal of Computational and Graphical Statistics* **25**, 1077–1096.

DEVINSKY, O. (1999). Patients with refractory seizures. *New England Journal of Medicine* **340**, 1565.

DURANTE, D. AND DUNSON, D. B. (2014). Nonparametric Bayes dynamic modelling of relational data. *Biometrika* **101**, 883–898.

EUÁN, C., OMBAO, H. AND ORTEGA, J. (2018). Spectral synchronicity in brain signals. *Statistics in Medicine* **37**, 2855–2873.

FELL, J. AND AXMACHER, N. (2011). The role of phase synchronization in memory processes. *Nature Reviews Neuroscience* **12**, 105–118.

FRIEDMAN, J., HASTIE, T. AND TIBSHIRANI, R. (2014). glasso: Graphical Lasso-estimation of Gaussian graphical models. R Package Version 1.8, available at https://CRAN.R-project.org/package=glasso.

FRISTON, K. (2009). Causal modelling and brain connectivity in functional magnetic resonance imaging. *PLoS Biology* **7**, 33.

FRISTON, K. J. (2011). Functional and effective connectivity: a review. *Brain Connectivity* **1**, 13–36.

FRISTON, K. J., HARRISON, L. AND PENNY, W. D. (2003). Dynamic causal modelling. *NeuroImage* **19**, 1273–1302.

GELMAN, A., STERN, H. S., CARLIN, J. B., DUNSON, D. B., VEHTARI, A. AND RUBIN, D. B. (2013). *Bayesian Data Analysis*. Boca Raton: Chapman and Hall/CRC.

GENG, J., BHATTACHARYA, A. AND PATI, D. (2018). Probabilistic community detection with unknown number of communities. *Journal of the American Statistical Association*, **114**, 893–905.

GOEBEL, R., ROEBROECK, A., KIM, D. S. AND FORMISANO, E. (2003). Investigating directed cortical interactions in time-resolved fMRI data using vector autoregressive modeling and Granger causality mapping. *Magnetic Resonance Imaging* **21**, 1251–61.

HOLMES, E. E., WARD, E. J. AND WILLS, K. (2012). Marss: multivariate autoregressive state-space models for analyzing time-series data. *R Journal* **4**, 11–19.

KALMAN, R. E. (1960). A new approach to linear filtering and prediction problems. *Transactions of the ASME Journal of Basic Engineering* **82**, 35–45.

KAMINSKI, M. AND BLINOWSKA, K. J. (1991). A new method of the description of the information flow in the brain structure. *Biological Cybernetics* **65**, 203–210.

KORZENIEWSKA, A., CRAINICEANU, C. M., KUŚ, R., FRANASZCZUK, P. J. AND CRONE, N. E. (2008). Dynamics of event-related causality in brain electrical activity. *Human Brain Mapping* **29**, 1170–1192.

KORZENIEWSKA, A., FRANASZCZUK, P. J., CRAINICEANU, C. M., KUŚ, R. AND CRONE, N. E. (2011). Dynamic of large-scale cortical interactions at high gamma frequencies during word production: event related causality (ERC) analysis of human electrocorticography (ECoG). *NeuroImage* **56**, 2218–2237.

KRAMER, M. A., TRUCCOLO, W., EDEN, U. T., LEPAGE, K. Q., HOCHBERG, L. R., ESKANDAR, E. N., MADSEN, J. R., LEE, J. W., MAHESHWARI, A., HALGREN, E. *and others*. (2012). Human seizures self-terminate across spatial scales via a critical transition. *Proceedings of the National Academy of Sciences of the United States of America* **109**, 21116–21121.

KRAMER, M. A., EDEN, U. T., CASH, S. S. AND KOLACZYK, E. D. (2009). Network inference with confidence from multivariate time series. *Physical Review E* **79**, 061916.

KUTSY, R. L., FARRELL, D. F. AND OJEMANN, G. A. (1999). Ictal patterns of neocortical seizures monitored with intracranial electrodes: correlation with surgical outcome. *Epilepsia* **40**, 257–266.

LITTLE, R. J. A. AND RUBIN, D. B. (2019). *Statistical Analysis with Missing Data*, New York: John Wiley & Sons, Inc.

MILO, R., ITZKOVITZ, S., KASHTAN, N., LEVITT, R., SHEN-ORR, S., AYZENSHTAT, I., SHEFFER, M. AND ALON, U. (2004). Superfamilies of evolved and designed networks. *Science* **303**, 1538–1542.

NEAL, R. M. AND HINTON, G. E. (1998). A view of the EM algorithm that justifies incremental, sparse, and other variants. In: Jordan, M. I. (ed.) *Learning in Graphical Models*. Cambridge, MA: The MIT Press, pp. 355–368.

NEWMAN, M. E. J. (2006). Modularity and community structure in networks. *Proceedings of the National Academy of Sciences of the United States of America* **103**, 8577–8696.

NICHOLSON, W. B., MATTESON, D. S. AND BIEN, J. (2017). Varx-l: structured regularization for large vector autoregressions with exogenous variables. *International Journal of Forecasting* **33**, 627–651.

NOWICKI, K. AND SNIJDERS, T. A. B. (2001). Estimation and prediction for stochastic blockstructures. *Journal of the American Statistical Association* **96**, 1077–1087.

POTTS, R. B. (1952). Spontaneous magnetization of a triangular Ising lattice. *Physical Review* **88**, 352.

RAMSAY, J. O. (2006). *Functional Data Analysis*. New York: Wiley Online Library.

SPORNS, O. (2011). *Networks of the Brain*. Cambridge, MA: The MIT Press.

SPORNS, O. (2013). Network attributes for segregation and integration in the human brain. *Current Opinion in Neurobiology* **23**, 162–171.

WENDLING, F., BARTOLOMEI, F., BELLANGER, J. J. AND CHAUVEL, P. (2002). Epileptic fast activity can be explained by a model of impaired GABAergic dendritic inhibition. *European Journal of Neuroscience* **15**, 1499–1508.

WITTEN, D. M., FRIEDMAN, J. H. AND SIMON, N. (2011). New insights and faster computations for the graphical lasso. *Journal of Computational and Graphical Statistics* **20**, 892–900.

WU, H., LU, T., XUE, H. AND LIANG, H. (2014). Sparse additive ordinary differential equations for dynamic gene regulatory network modeling. *Journal of the American Statistical Association* **109**, 700–716.

XUE, H., MIAO, H. AND WU, H. (2010). Sieve estimation of constant and time- varying coefficients in nonlinear ordinary differential equation models by considering both numerical error and measurement error. *The Annals of Statistics* **38**, 2351–2387.

ZHANG, T., SUN, Y., LI, H., YAN, G., TANABE, S., MIAO, R., WANG, Y., CAFFO, B. AND QUIGG, M. (2019). Bayesian inference of a directional brain network for intracranial EEG data. *Computational Statistics and Data Analysis*, 106847.

ZHANG, T., WU, J., LI, F., CAFFO, B. AND BOATMAN-REICH, D. (2015). A dynamic directional model for effective brain connectivity using electrocorticographic (ECoG) time series. *Journal of the American Statistical Association* **110**, 93–106.

ZHANG, T., YIN, Q., CAFFO, B., SUN, Y. AND BOATMAN-REICH, D. (2017). Bayesian inference of high-dimensional, cluster-structured ordinary differential equation models with applications to brain connectivity studies. *The Annals of Applied Statistics* **11**, 868–897.

[*Received February 19, 2019; revised November 26, 2019; accepted for publication November 29, 2019*]